Bioinspired Adhesives

Houwen Matthew Pan, Nanyang Technological University, Singapore, Singapore

1 Introduction

Animals such as geckos, flies, spiders, and beetles possess the ability to rapidly attach and detach from varied surfaces under highly diverse conditions [1–4]. This unique ability has garnered the attention of scientists and through modern imaging techniques, detailed examination of their attachment pads was carried out and revealed a complex hierarchical structure consisting of fibers, that span the millimeter to nanometer range. These hairs have characteristic geometries, sizes, and mechanical properties depending on the animal. In the example of the gecko, keratinous hairs (setae) are 30–130 mm in length and split up into smaller nanometer-sized spatula-shaped structures (Fig. 1) [5]. Inspired by the complex yet rational organization of nature's adhesive structures, a wide array of fabrication techniques has been applied to recreate their hierarchical adhesive structures [6].

Besides innovations in fabrication methods, huge strides have also been made theoretically. Van der Waals interactions generated by contacting fibers (spatulae) have been discovered to be the key to their adhesive ability [7,8] and contact mechanics theory by Johnson–Kendal–Robert (JKR) [9] applied to further explain the adhesion properties of fibrillar structures and the parameters that influence them [10–12]. With scientific advances made in both experimental and theoretical research for bioinspired adhesives, a range of applications has been proposed. These include wall-climbing robots [13,14], synthetic dry adhesives for space applications [15], reusable adhesive tapes [16], transfer printing [17], locomotion [18], and medical skin patches [19].

This review paper discusses design parameters that were found to be instrumental to the adhesive properties of synthetically fabricated adhesive structures, currently available fabrication methods for producing these adhesive structures, as well as the various testing methods that have been used experimentally to characterize adhesion performance. A table summarizing the types of material used, young's modulus, fabrication methods, structure, dimensions, adhesion testing methods, adhesion strength of published literature from 2008 to 2019 is provided in the review. In the final section, current trends, challenges and future outlook of the field of bioinspired adhesives are discussed. This review aims to summarize and organize the vast scientific knowledge accumulated and will serve to be an interesting read for material scientists, theoretical physicists, chemists and all other researchers interested in the field of bioinspired adhesives.

2 Design Parameters

The design of bioinspired dry adhesives is geometry dominated [20,21] and is highly dependent on the material properties, contact radius and shape, aspect ratio, and orientation of individual fibers as well as the geometry and hierarchical arrangement of the fiber array.
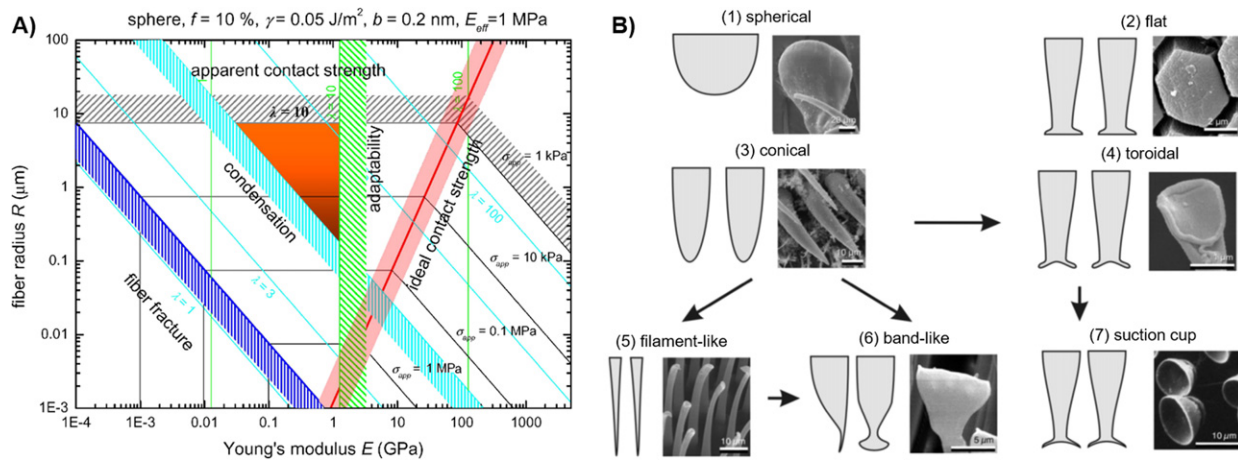
Fig. 1 The hierarchical structures of Gekko gecko. A gecko toe contains hundreds of thousands of setae and each seta contains hundreds of spatulae. ST: seta; SP: spatula; BR: branch. Reproduced with permission from Gao, H., Wang, X., Yao, H., Gorb, S., Arzt, E., 2005. Mechanics of Materials 37 (2), 275–285. Copyright 2005 Elsevier.

2.1   Material Properties

The mechanical stability and surface energy of fibers are key to successful design of synthetic adhesives. Van der Waals forces are the main adhesion component in gecko's dry adhesion (~10 N/cm^2) [8,22–24]. However, recent studies have pointed out that besides van der Waals interactions, capillary forces also play a major role in the dry adhesion ability of geckos [25,26]. Long fibers are mechanically unstable as they collapse under their own weight and clump together if adhesive forces between fibers are greater than bending forces, this in turn reduces the contact area and decreases overall adhesion of the fiber array. For this reason, fibers should be made of materials of high Young's modulus such as β-keratin (2–4 GPa) which is the material that gecko hair fibers ('setae') are made from. The mechanical behavior of gecko setae was thoroughly studied by Autumn *et al.* [27] and Peattie *et al.* [28] Furthermore, stiff microfibrillar structures are less prone to wear and should preserve their adhesive properties for longer durations. However, fibers that are too stiff will lose their ability to deform elastically, leading to a decrease in adhesive contact area.

The optimal adhesive design in terms of fiber height, thickness, elasticity, and spacing are represented visually on an adhesion map (**Fig. 2(A)**) [11]. Fibers should be stiff enough to not fracture before detachment (fiber fracture limit). At the point of tensile instability, the ideal contact strength transmitted through the contact area should be more than the contact strength (ideal contact strength limit). Fibers should not clump and form bundles during bending (condensation limit). For proper adhesion to rough surfaces, fibers should have a minimum elastic adaptability (adaptability limit).

2.2   Contact Radius and Shape

Another important design parameter is the fiber's contact radius and shape. The various contact shapes found in animals includes spherical, conical, flat, or toroidal, just to name a few (**Fig. 2(B)**) [29]. Amongst them, flat contact fibers demonstrate the highest adhesion to smooth surfaces, however its adhesive capability declines rapidly with the presence of roughness or dirt and hence it not suitable for real life applications. Interestingly, animals with highly elastic fibers tend to have flat contact fiber tips, whereas animals with stiffer fibers adopt torus or band-like contact shapes to accommodate for their lack of elasticity.

In their study, Arzt *et al.* compared pillars with different contact shapes, and discovered that reducing contact radius and/or increasing fiber length has a profound influence on adhesion behavior [30]. Based on JKR contact mechanics theory, the division of a contact area into a number of smaller elements, n, amplifies adhesion by a factor of n^r. The exponent r is referred to as 'splitting efficiency' and varies according to contact geometry [29]. This principle has been named 'contact splitting' and provides a quantitative explanation for why lighter animals such as flies have a lower density of hairs on their attachment pads than heavier animals such as geckos [7]. Arzt *et al.* further discovered that tip geometry has a strong impact on adhesion strength [31,32]. For example, fibers with mushroom-shaped contacts were found to improve stress distribution within the area of contact, leading to an increase in adhesion [33,34].

2.3   Fiber Aspect Ratio and Orientation

Fiber aspect ratio has a strong influence on the effective material property of individual fibers. Fiber microarrays of high aspect ratios (long and thin) have a significantly lower effective modulus as compared to fibers of lower aspect ratios [35]. Fiber aspect ratios are highly dependent on fabrication methods [11].
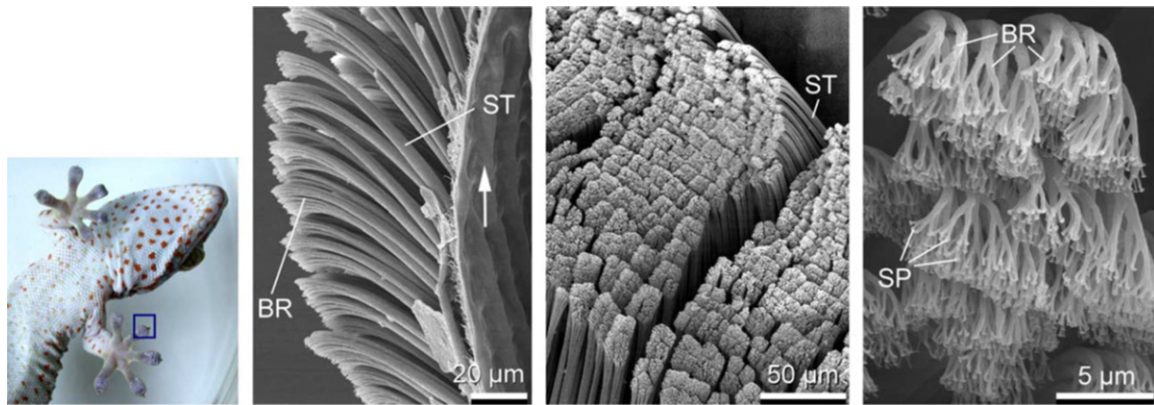
Fig. 2 (A) Adhesion map for spherical tip contacts with the follow parameters: work of adhesion, $\gamma = 0.05$ J/m^2, area fraction of fibers, f = 10%, characteristic length of surface interaction, b = 0.2 nm. The criteria for fiber fracture (blue line), ideal contact strength (red line), condensation (cyan lines) and adaptability (green lines) are indicated. The triangular target area delineates the allowed parameter space for an adhesive structure of aspect ratio $\lambda = 10$ and apparent contact strength of at least 1 kPa. (B) Contact shapes of attachment devices in nature and their hypothetical evolution paths (shown as arrows). (1) Bug Pyrrhocoris apterus, smooth pulvillus. (2) Grasshopper Tettigonia viridissima, surface of the attachment pad. (3) Fly Myathropa florea, unspecialized hairs on the leg. (4) Fly Calliphora vicina, seta of the pulvilli. (5) Beetle Harmonia axyridis, seta of the second tarsal segment. (6) Beetle Chrysolina fastuosa, seta of the second tarsal segment. (7) Male beetle Dytiscus marginatus, suction cups on the vertical side of the foreleg tarsi. Reproduced with permission from (A) Spolenak, R., Gorb, S., Arzt, E., 2005. Acta Biomaterialia 1 (1), 5–13. (B) Spolenak, R., Gorb, S., Gao, H., Arzt, E., 2005. Proceedings of the Royal Society A: Mathematical, Physical and Engineering Sciences 461 (2054), 305–319. Copyright 2005 Elsevier.

Fibers' orientation with respect to the surface (tilt angle) is an important albeit less studied design parameter in fabrication of dry adhesives. Studies involving tilted fibers of high aspect ratio demonstrated anisotropic shear adhesion, an interesting feature for synthetic adhesives to avoid peeling off when subjected to shear stress [36,37].

2.4 Geometry of Fiber Array

Fiber packing symmetry is another important design consideration. Most geckos have a setae arrangement of square arrays to avoid clumping of fibers [38]. A hexagonal fiber arrangement would provide maximum adhesion performance due to the high number of fibers that are in contact but could lead to severe clumping of fibers when inter-fiber distance decreases. Besides isotropic array designs, complex anisotropic material designs are frequently found in natural attachment systems [39,40] and could open the path for more sophisticated adhesion geometries [41].

2.5 Hierarchy

The best example of structural hierarchy is demonstrated by the Tokay gecko's foot, starting from lamellae in the millimeter scale, which are divided into arrays of millions of fine microscopic setae, 110 μm in height and 5 μm in diameter, and further splitting into hundreds of nanometer-sized spatulae, 2 μm in height and 200 nm in diameter [6].

3 Fabrication Methods

Different methods of fabrication adhesive structures have been organized and categorized into five main approaches: (1) Microfabrication techniques such as photolithography, electron beam lithography, or dry etching, (2) soft molding of elastomeric polymers, (3) capillary force lithography, (4) filling of porous membranes, (5) chemical vapor deposition, and (6) large-scale manufacturing technologies. A non-exhaustive list of dry adhesive structures fabricated from different methods is given in **Table 1**. The table summarizes key publications from 2008 to 2019 pertaining to the field of bioinspired dry adhesives.

3.1 Microfabrication

The fabrication of high quality molds or templates is the most important prerequisite for lithography-based techniques. These are typically made of silicon via dry etching or by deposition of metals on patterned substrates.

Fiber microarrays can also be produced directly via microfabrication techniques such as photolithography and dry etching. With this approach, hierarchical structures are produced with fibers that were 250 nm in diameter and 4 mm in height, mimicking the structure of the gecko setae [42,43]. In another study, fiber microarrays made from poly(imide) (PI) were fabricated using e-beam lithography and pattern transfer by dry etching in oxygen plasma [43]. This microfabrication method produced fibers that

Table 1 A non-exhaustive list of synthetic dry adhesives produced from different materials and fabrication methods. PP – poly(propylene), PE – poly(ethylene), PUA – poly(urethane acrylate), PDMS – Poly(dimethylsiloxane), CNT – carbon nanotube, Pth – poly(thiophene), PVS – poly(vinylsiloxane), PMMA - poly(methyl methacrylate), PC – poly(carbonate), PS – poly(styrene), AA – anodic aluminum, AFM – atomic force microscope, d – diameter, s – spacing, h – height

Material	Young's modulus	Fabrication method	Structure and shape	Dimensions @ highest level (μm)	Adhesion test	Adhesion strength	Refs.
PDMS	1.75 MPa	Soft molding of PDMS on SU-8 templates fabricated from photolithography	Wedge shaped fibers	d = 20 or 50, h = 80 or 200	Flat contact (glass surface)	5.1 kPa (normal) 17 kPa (shear)	[67]
PDMS	2.4–3.0 MPa	Soft molding of PDMS on aluminum alloy templates	Three-tier cylindrical pillar structure	d = 300, s = 600, h = 1200	Flat contact (glass substrate)	/w mushroom tip: ~43.6 kPa (normal) w/o mushroom tip: ~18.0 (normal)	[75]
PDMS	–	Soft molding of PDMS on Si templates followed by bonding of fiber array via dip-transfer	PDMS nanofibers on top of tilted micropillars	d = 10, s = 20, h = 5	Flat contact (Si surface)	2.35 N/cm^2 (normal) 5.96 N/cm^2 (shear)	[76]
PDMS	–	Soft molding of PDMS on Si templates fabricated from photolithography and dry etching	Wide-tip micropillars	d = 5, s = 20, h = 10	Flat contact (silicone surface)	10.3 N/cm2 (normal)	[77]
PDMS	1.5 MPa	Soft molding of PDMS on templates fabricated from photolithography followed by thermal treatment	Micropillar arrays	d = 19, s = 40, h = 13	Flat contact (Si surface)	7.09 mN (normal)	[78]
PDMS-g-poly(n-butyl acrylate) (PDMS-g-PBA)	1.51 MPa	Soft molding of PDMS on PU templates to form pillars, dip transfer to form mushroom tips then grafting of PBA chains	Mushroom-shaped pillars grafted /w PBA chains	d = 52, s = 125, h = 106	Hemispherical contact (colloidal probe-AFM, d = 6 mm)	~14 mN (normal)	[65]
poly(glycerol-co-sebacate acrylate) (PGSA)	0.38 MPa	Soft molding of PGSA on Si template fabricated from photolithography and dry etching	Conical microfibers	d = 0.18, s = 2.7, h = 2.4	Macroscale shear test	4.8 N/cm^2 (shear)	[16]
PU	3 MPa	Soft molding of PU from silicone templates fabricated by lithography followed by dip transfer	Tilted microfibers with angled mushroom tips	d = 35, s = 120, h = 100	Hemispherical contact (colloidal probe-AFM, d = 6 mm) Macroscale shear test	~5 mN (normal) ~32 mN (shear) 100 kPa (shear)	[71]
PU	–	Soft molding of PU on Si templates fabricated from photolithography and dry etching.	Nanofibers with spatula tips	d = 0.41, h = 2	Flat contact (Si disk)	14.1 N/cm^2 (normal)	[79]
PU	25 MPa	Soft molding of PU on PDMS templates fabricated from photolithography.	Rectangular tips on top of tilted prismatic pillars	d = 20 × 7 (rectangular face), s = 37, h = 20	Macroscale shear test	1.25 N/cm^2 (normal) 2.8 N/cm^2 (shear)	[80]
PUA nanocomposites (15%Fe$_3$O$_4$ NPs /w SiO$_2$ shells)	20–110 MPa	Soft molding of PUA nanocomposites on Si templates.	Tilted gradient pillars	d = 2.5, s = 6, h = 20	Hemispherical contact (colloidal probe-AFM, d = 4 mm) Macroscale shear test	25.1 mN (shear) ~8 mN (normal) 8.8 N/cm^2 (shear)	[81]
PVS	–	Soft molding of PVS on templates followed by plasma treatment	Mushroom-shaped micropillars	d = 40, h = 70	Hemispherical contact (colloidal probe-AFM, d = 3 mm)	28.9 mN (normal)	[82]
NOA81	1.36 GPa	Soft molding of NOA81 on AZ P4620 templates fabricated from photolithography.	Mushroom-shaped tips on top of vertical or tilted pillars	d = 0.5, h = 1.0	Macroscale shear test	7 or 8.5 N/cm^2 (shear)	[83]
PC	2 GPa	Capillary force assisted nanoimprinting using a porous AA template	Pillars splitting into multiple fibers	d = 0.09, h = 0.85	Macroscale shear test	6.5 N/cm^2 (shear)	[84]

Material	Modulus	Fabrication method	Structure	Dimensions (μm)	Test	Adhesion	Ref
PS	3.2 GPa	Filling of porous AA membrane with melted PS	Pillars splitting into multiple fibers	d = 70, h = 200–700	Hemispherical contact (colloidal probe-AFM, d = 24 μm)	~1.1 μN (normal) ~8 μN (shear)	[85]
PP	1 GPa	Filling of porous PC membrane with melted PP	Microfiber array	d = 0.6, h = 20	Macroscale Shear test	2 N/cm^2 (shear)	[86]
PP	1.5–2 GPa	Filling of porous PC membrane with melted PP	Tilted nanofibers on top of micropillars	d = 0.6, s = 2.77	Hemispherical contact (colloidal probe-AFM, d = 30 μm)	326 nN (normal)	[87]
High density PE (HDPE)	0.9 GPa	HDPE patterned by laser ablation and melted into porous PC membrane.	Nanofiber array on top of lamellar flaps	d = 0.6, h = 18	Macroscale shear test	2.5 N/cm^2 (shear)	[88]
PE	0.4–1 GPa	Filling of porous PC membrane with melted PE	Tilted nanofibers on top of micropillars	d = 0.6	Hemispherical contact (colloidal probe-AFM, d = 30 μm)	254 nN (normal)	[89]
Pth	1.5 GPa	Electrochemical deposition of Pth on porous AA membrane	Nanotubule arrays	d = 0.2, h = 8–20	Flat contact (glass surface) Macroscale shear test	80 N/cm^2 (normal) 174 N/cm^2 (shear)	[90]
Teflon	1.5 GPa	Filling of porous AA membrane with melted Teflon	Double-level Teflon nanopillars	d = 0.2, h = 37	Hemispherical contact (colloidal probe-AFM, d = 8 mm)	1.1 N/cm^2 (normal) 12 N/cm^2 (shear)	[91]
Teflon	1.5 GPa	Filling of porous AA membrane with melted Teflon	Fluffy nanostructure on top of each nanopillar	d = 0.2, h = 16	Hemispherical contact (colloidal probe-AFM, d = 6 mm)	7 mN (normal)	[92]
PMMA	–	Capillary force lithography using PUA mold	Lotus leaf-like surfaces	d = 0.15, s = 0.2, h = 0.5	Hemispherical contact (colloidal probe-AFM, d = 500 μm)	Coefficient of friction = 0.65	[93]
PDMS	4–5 GPa	Capillary force lithography	Micropillars on top of large pillars	d = 1, s = 2, h = 1	–	–	[94]
CNTs	–	CVD	Vertically aligned nanofibers	d = 150, h = 0.01–0.015	Macroscale shear test	100 N/cm^2 (shear) 20 N/cm^2 (normal)	[54]
CNTs	1 TPa	CVD	Brush-like CNTs	d = ~0.008, h = 700–1000	Macroscale shear test	44.5 N/cm^2 (shear)	[95]
CNTs	4 GPa (SU-8)	VA-CNTs grown by CVD and imprinted on top of SU-8 micropillars	SU-8 vertical pillars supporting VA-CNTs	d = 0.02, h = 20	Hemispherical contact (colloidal probe-AFM, d = 1 mm)	0.5 mN (normal) 0.88 mN (shear)	[96]
Ge nanowires /w parylene shell	100–150 GPa	Ge nanowires grown by CVD followed by parylene coating	Non-aligned nanowires	d = 0.02–0.03, h = 30	Macroscale shear test	163 N/cm^2 (shear)	[58]
Nickel and photoresist	6.2 GPa	Nano/microstructures created from photolithography & dry etching, followed by plasma treatment	Nickel paddles supporting vertically aligned polymer nanorods	d = 0.2, h = 3	Flat contact (glass punch)	14 Pa (normal)	[97]
Acrylic based negative tone resist (IPG780)	4 GPa	3D direct laser writing	Mushroom-shaped fibers on micropillars	d = 0.6, s = 1.1 or 1.4, h = 1.0 or 2.7	Hemispherical contact (colloidal probe-AFM, d = 20 μm)	~0.12 μN (normal)	[98]

were 0.2–4 mm in diameter and 0.15–2 mm in height with adhesion performance similar to that of the gecko's dry adhesion ability.

3.2 Soft Molding

Soft molding of UV curable elastomeric precursors such as poly(dimethylsiloxane) (PDMS) on microfabricated molds is a popular technique for producing regular arrays of micropillars (Fig. 3(A) and (B)) [44–47]. After photocuring, the elastomeric replica can be easily separated from the mold due to the chemical inertness of PDMS. This approach has been used to produce regular patterns at high fidelity to study the influence of design parameters such as pillar aspect ratios [44] and contact radius [30] on final adhesion strength. Microarrays of pillars with spatula, spherical, and suction cup tips were fabricated using a modified soft molding approach [32].

3.3 Capillary Force Lithography

Soft molding of fiber arrays is performed with soft polymeric materials with limited mechanical strength. This leads to low aspect ratios of fabricated pillars as collapse occurs for higher aspect ratios due to the material's low mechanical stability. In order to use rigid polymeric materials of higher mechanical strength, a different fabrication method is required. In capillary force lithography, thermoplastic materials are typically patterned by hot-embossing which involves flowing a polymer melt through micro or
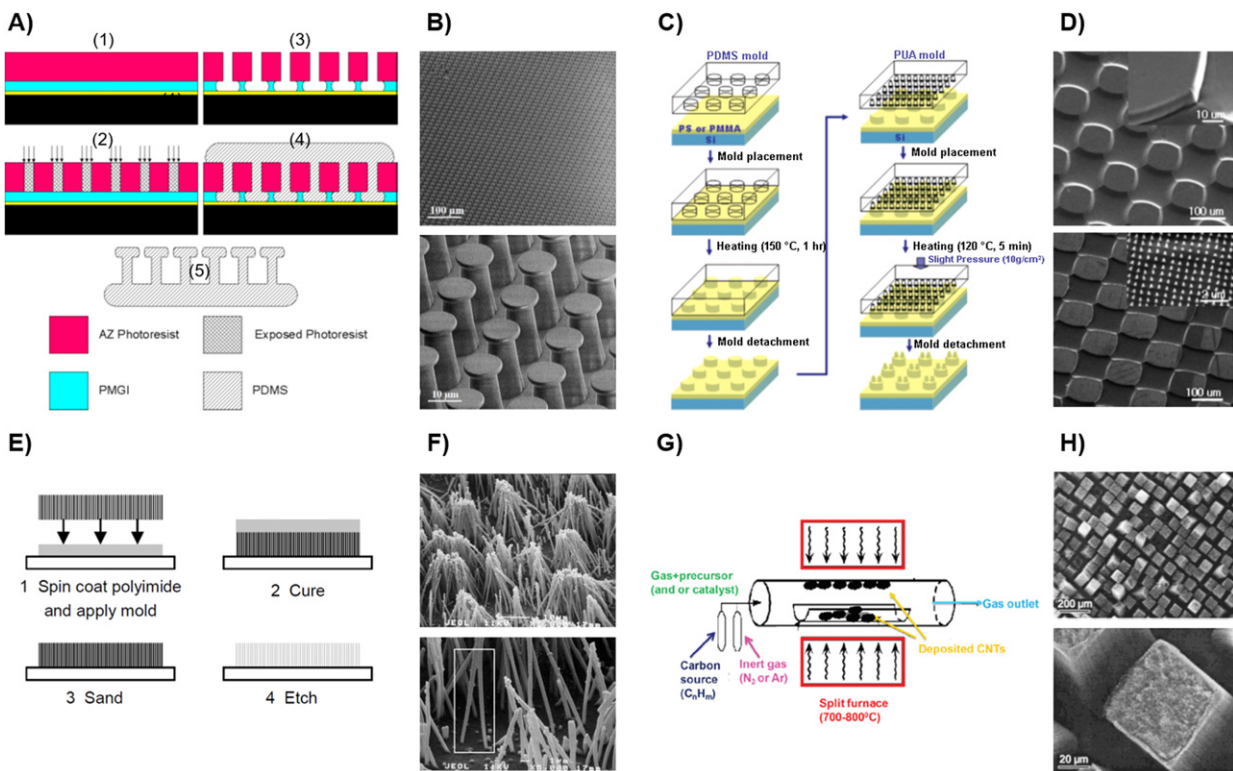

Fig. 3 (A) (1) A silicon wafer is coated with Cr/Au followed by spin-coating and baking PMGI and AZ 9260 photoresists. (2) The AZ 9260 is UV-exposed under the post array mask. (3) Following exposure, the photoresist is developed and dried, leaving undercut areas. (4) Sylgard® 184 is poured onto the mold and cured. (5) The cured silicone is removed by hand, producing the final dry adhesive. (B) SEM images of 10 μm diameter posts with a cap thickness of 1.5 μm and post height of ~ 20 μm. (C) Schematic of the two-step capillary force lithography process. Polymer microstructures were fabricated using a micropatterned PDMS mold followed by nanofabrication on top of the preformed microstructure using a nanopatterned PUA mold. (D) SEM images of PS microstructures and micro/nanoscale hierarchical structures. A microstructure with 120 μm posts and 25 μm spacing was used. The nanostructure is 100 nm in diameter and 400 nm in spacing with a height of 450 nm. (E) Synthetic fiber fabrication by nanocasting. (F) Clumping in an array of 0.6 μm diameter polyimide fibers. (G) Schematic diagram of chemical vapor deposition (CVD) setup. (H) SEM images of MWCNTs deposited on a masked pattern after 10 min of CVD. Reproduced with permission from (A, B) Sameoto, D., Menon, C., 2009. Journal of Micromechanics and Microengineering 19 (11), 115002. (D) Jeong, H.E., Lee, S.H., Kim, J.K., Suh, K.Y., 2006. Langmuir 22 (4), 1640–1645. Copyright 2006 American Chemical Society. (F) Majidi, C., Groff, R., Fearing, R., 2004. Proceedings of the International Mechanical Engineering Congress and Exposition (IMECE), pp. 579–584. California. (G) Khan, W., Sharma, R., Saini, P., 2016. Carbon Nanotubes – Current Progress of Their Polymer Composites. InTech. (H) Delzeit, L., Nguyen, C.V., Chen, B., et al., 2002. The Journal of Physical Chemistry B 106 (22), 5629–5635. Copyright 2002 American Chemical Society.

nanostructured molds under specific heat and pressure processing conditions. Besides pressure and temperature, the filling also depends on viscosity of polymer melt, hydrophobicity of mold, and pattern geometry. Solidification of polymer melt is achieved by cooling below the crystallization or glass transition temperature of semicrystalline or amorphous polymers, respectively. The final step involves either peeling off or selective dissolution of the template to release the polymer that has solidified in the geometry of the template. This fabrication method has been used to produce arrays of poly(methyl methacrylate) (PMMA) pillars that are 150 nm in diameter and up to 500 nm in height, using a polyurethane acrylate mold [48]. Through a two-step temperature-directed capillary molding process, hierarchical structures of micro- and nanometer-sized pillars of various sizes and spacings were obtained (Fig. 3(C) and (D)) [49]. For this approach, only superhydrophobicity was demonstrated, surface adhesion is yet to be tested.

3.4   Filling Porous Membranes

Due to the time-consuming and costly microfabrication process required to produce high quality molds, cheaper alternatives such as porous polycarbonate (PC) and anodic alumina (AA) membranes have been utilized in the production of arrays of long, nanometer-sized fibers [50,51]. These membranes are commercially available with micrometre- or nanometer-sized pores with different inter-pore spacings and membrane thicknesses. Porous PC membranes containing 0.6 μm cylindrical pores with spacings of less than 5 mm were filled with PI solutions to produce dense arrays of high aspect ratio nanofibers (Fig. 3(E) and (F)) [38].

3.5   Chemical Vapor Deposition (CVD)

Chemical vapor deposition (CVD) is an alternative fabrication technique that does not require a template. Arrays of vertically aligned carbon nanotubes (CNTs) is one of the most popular form of dry adhesive fabricated via CVD (Fig. 3(G) and (H)) [52,53]. CNTs produced from this method possess superior mechanical strength and is able to achieve ultra high aspect ratios [54]. Although adhesion strengths were reported to be 200 times greater than that of geckos, the values correspond to a single bundle of CNTs and not representative of the entire array [55]. The high temperature requirement for CVD fabrication of CNTs makes it impossible for direct fabrication on polymers, severely limiting their sample size (<1 cm^2) [56]. For most applications, rigid surfaces have been used. Other studies on CNT-adhesives examined the effect of water on the adhesive surface and demonstrated that they collapse complete when exposed to water. Other gas phase growth methods include the use of parylene, a gas-deposited polymer, grown on nanofibers containing either a carbon [57] or germanium [58] core.

3.6   Large-Scale Manufacturing Technologies

Most fabrication techniques available for creating synthetic dry adhesives are limited only to the laboratory and is severely lacking in terms of scalability and productivity. As such, efforts in the past 5 years have been focused on establishing continuous and scalable production processes. Arzt et al. developed a roll-to-roll process for fabrication of high-performance, mushroom-shaped dry adhesives out of micropatterns made from UV-curable PU acrylates [59]. A thermal roll-imprinting lithography (TRL) system was designed by Kwak et al. for the continuous production of PDMS microstructures [60]. Jeong et al. introduced a manufacturing technique based on automated CNC machining and replica molding that enables simple and scalable fabrication of bioinspired dry adhesives [61].

4   Adhesion Tests

Due to the lack of standardized adhesion testing methods in the field, there has been a huge range of adhesion properties reported in recent years. Three main types of adhesion tests are shown in Fig. 4. Flat contact tests, hemispherical contact tests and shear measurements or peel tests. Flat and hemispherical contact tests are typically designed to quantify normal adhesion strength of isotropic dry adhesives. Shear measurements of peel tests can be used to characterize anisotropic dry adhesives.

4.1   Flat Contact

Flat–flat contact adhesion tests are able to provide a well-defined contact area and give accurate results for measurements involving normal adhesion pressure. However, precise alignment of contact devices is crucial to produce accurate results and a self-aligning mechanism may be employed. Typically, there are two variations of this testing method: the rigid adhesive sample is pulled off a flat contact surface (Fig. 4(A)) [62,63] or a flat contact surface is pulled off the adhesive sample (Fig. 4(B)) [64].

4.2   Hemispherical Contact

In contrast to the flat contact approach, the hemispherical contact adhesion test does not require precise alignment during adhesion testing and does not have a fixed contact area – contact area is dependent on the preload. The hemispherical contact is
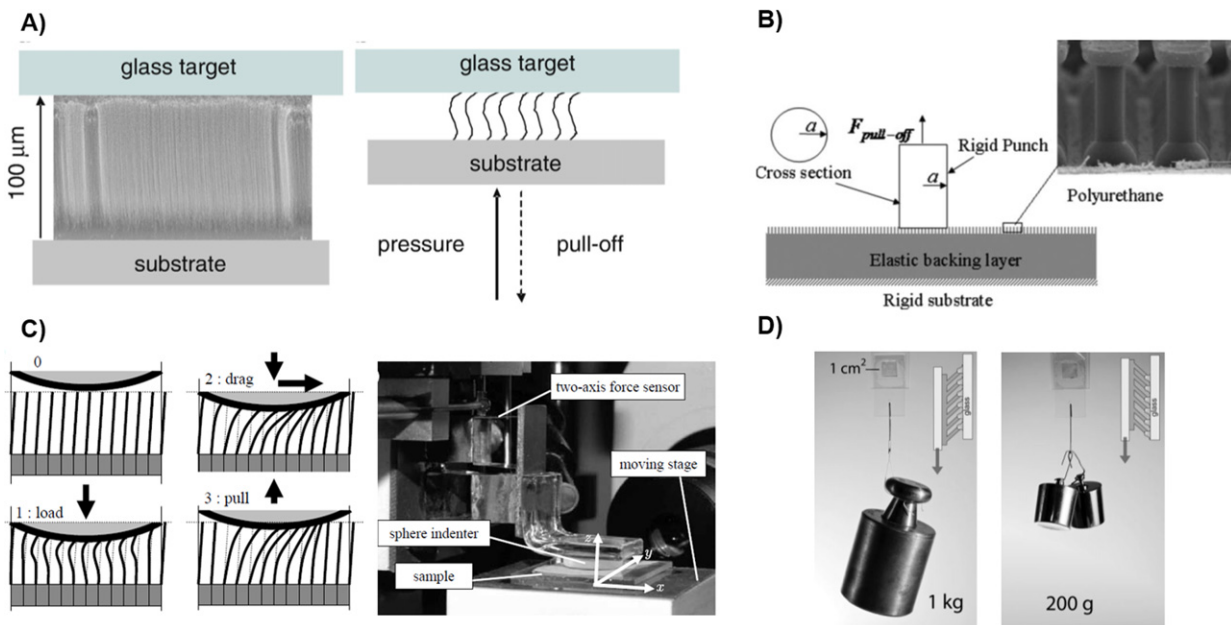
Fig. 4 Schematic representation of flat-flat contact adhesion measurement. (A) The adhesive sample was manually pressed (100 N) against a glass surface, and subsequently pulled off. The force was measured with a spring balance. (B) A flat punch is pressed down on microfiber arrays with spatulated tips. An inverted microscope is used to observe the contact area during the measurements. (C) (left) Path of hemispherical contact probe during LDP test on fiber array. (right) Two-axis normal and shear force sensor. (D) Polyurethane fiber microarray with 14° angled tips adhering to smooth glass was able to support ~100 kPa in shear in the gripping direction but only ~20 kPa in the releasing direction. Reproduced with permission from (A) Wirth, C.T., Hofmann, S., Robertson, J., 2008. Diamond and Related Materials 17 (7), 1518–1524. Copyright 2008 Elsevier. (B) Long, R., Hui, C.-Y., Kim, S., Sitti, M., 2008. Journal of Applied Physics 104 (4), 044301. Copyright 2008 American Institute of Physics. (C) Schubert, B., Lee, J., Majidi, C., Ronald, R.S., 2008. Journal of the Royal Society Interface 5 (25), 845–853. (D) Murphy, M.P., Aksak, B., Sitti, M., 2009. Small 5 (2) 170–175. Copyright 2009 Wiley.

widely used in adhesion testing due to its immense versatility to different applications [65,66]. Higher adhesive forces are measured with lightly preloaded hemispherical tips as the contact area closely resembles that of a flat surface in this region. Peel force measurements can also be made by attaching fibers to areas of hemispheric contact that are curved away from the adhesive surface, For testing anisotropic adhesive samples, both the flat–flat [36,67] and hemispherical tip contacts [68] have been used in a test method known as load–drag–pull (LDP) (**Fig. 4(C)**) where a normal load is applied, followed by tangential displacement, then measurement of pull-off force.

4.3   Shear Measurements or Peel Tests

Shear and peel strength measurements are typically macroscale measurements and require larger adhesive samples. Shear strength measurements are frequently used to characterize CNT-based adhesives, which have small normal adhesion strengths, and also in testing anisotropic adhesives (**Fig. 4(D)**) [69–71]. For shear adhesion tests, no normal load is applied to the material.

The peel test is frequently applied to test the peel strength of elastomers [72], and to test both isotropic [73], and anisotropic dry adhesives [74]. The theoretical model for thin film peeling can be applied to derive adhesion energy and compared with those of unstructured polymers. In this model, factors such as young's modulus, sample thickness and width are all taken into account.

5   Conclusion and Outlook

With advances made in fabrication techniques, the reproducible production of complex hierarchical structures is now possible. Especially promising are soft elastomeric polymers as materials for synthesis of dry adhesives and have been demonstrated to be compatible with large-scale manufacturing techniques such as roll-to-roll UV lithography, thermal roll-imprinting lithography, and CNC machining and replica molding. Another exciting approach for synthetic adhesives is the fabrication of high density arrays of vertically aligned CNTs (VA-CNTs). CNTs are superior mechanically and can be produced at exceptionally high aspect ratios (>1000:1) without buckling due to their superior mechanical properties and have been demonstrated to have excellent adhesive properties, perhaps even greater than that of the gecko's. Recent efforts have also seen the incorporation of advanced features such as mushroom-shaped structures to improve contact stress distribution and adhesion directionality to facilitate detachment.

However, with current bioinspired dry adhesives, the long-term sustainability of adhesive properties and adaptability to different surface conditions and unpredictable environmental factors remain as questions to be answered. A smaller concern for the field of synthetic dry adhesives is the development of standardized testing methods to facilitate direct comparison of published results. Also, results from nano- and microscale adhesion tests are largely inadequate for the characterization of macroscale performance and macroscale testing methods should play a bigger role in quantifying performance of synthetic adhesives.

In conclusion, scientists in the field of bioinspired adhesives have a challenging task ahead but once these problems are solved synthetic adhesives are expected to play an enabling role for a wide range of adhesive products from household devices such as reusable adhesive tapes to high-end applications such as wall-climbing robots in outer space.

References

[1] Autumn, K., Liang, Y.A., Hsieh, S.T., et al., 2000. Adhesive force of a single gecko foot-hair. Nature 405, 681.

[2] Gorb, S., Gorb, E., Kastner, V., 2001. Scale effects on the attachment pads and friction forces in syrphid flies (Diptera, Syrphidae). Journal of Experimental Biology 204 (8), 1421–1431.

[3] Ritzmann, R.E., Gorb, S., Quinn, R.D., 2004. Arthropod locomotion systems: From biological materials and systems to robotics. Arthropod Structure & Development 33 (3), 183–185.

[4] Peattie, A.M., Autumn, K., 2002. Mechanisms of adhesion in geckos1. Integrative and Comparative Biology 42 (6), 1081–1090.

[5] Gao, H., Wang, X., Yao, H., Gorb, S., Arzt, E., 2005. Mechanics of hierarchical adhesion structures of geckos. Mechanics of Materials 37 (2), 275–285.

[6] Jeong, H.E., Suh, K.Y., 2009. Nanohairs and nanotubes: Efficient structural elements for gecko-inspired artificial dry adhesives. Nano Today 4 (4), 335–346.

[7] Arzt, E., Gorb, S., Spolenak, R., 2003. From micro to nano contacts in biological attachment devices. Proceedings of the National Academy of Sciences of the United States of America 100 (19), 10603–10606.

[8] Autumn, K., Sitti, M., Liang, Y.A., et al., 2002. Evidence for van der Waals adhesion in gecko setae. Proceedings of the National Academy of Sciences of the United States of America 99 (19), 12252–12256.

[9] Johnson, K.L., Kendall, K., Roberts, A.D., Tabor, D., 1971. Surface energy and the contact of elastic solids. Proceedings of the Royal Society of London. A. Mathematical and Physical Sciences 324 (1558), 301–313.

[10] Gu, Z., Li, S., Zhang, F., Wang, S., 2016. Understanding surface adhesion in nature: A peeling model. Advanced Science 3 (7), 1500327.

[11] Spolenak, R., Gorb, S., Arzt, E., 2005. Adhesion design maps for bio-inspired attachment systems. Acta Biomaterialia 1 (1), 5–13.

[12] Jagota, A., Hui, C.-Y., 2011. Adhesion, friction, and compliance of bio-mimetic and bio-inspired structured interfaces. Materials Science and Engineering: R: Reports 72 (12), 253–292.

[13] Daltorio, K.A., Gorb, S., Peressadko, A., et al., 2011. Microstructured polymer adhesive feet for climbing robots. MRS Bulletin 32 (6), 504–508.

[14] Aksak, B., Murphy, M.P., Sitti, M., 2008. Gecko inspired micro-fibrillar adhesives for wall climbing robots on micro/nanoscale rough surfaces. In: Proceedings of the 2008 IEEE International Conference on Robotics and Automation, pp 3058–3063.

[15] Menon, C., Lan, N., Sameoto, D., 2009. Towards a methodical approach to implement biomimetic paradigms in the design of robotic systems for space applications. Applied Bionics and Biomechanics 6 (1), 87–99.

[16] Mahdavi, A., Ferreira, L., Sundback, C., et al., 2008. A biodegradable and biocompatible gecko-inspired tissue adhesive. Proceedings of the National Academy of Sciences of the United States of America 105 (7), 2307–2312.

[17] Sariola, V., Sitti, M., 2014. Mechanically switchable elastomeric microfibrillar adhesive surfaces for transfer printing. Advanced Materials Interfaces 1 (4), 1300159.

[18] Zhou, M., Tian, Y., Sameoto, D., et al., 2013. Controllable interfacial adhesion applied to transfer light and fragile objects by using gecko inspired mushroom-shaped pillar surface. ACS Applied Materials & Interfaces 5 (20), 10137–10144.

[19] Kwak, M.K., Jeong, H.-E., Suh, K.Y., 2011. Rational design and enhanced biocompatibility of a dry adhesive medical skin patch. Advanced Materials 23 (34), 3949–3953.

[20] Brodoceanu, D., Bauer, C.T., Kroner, E., Arzt, E., Kraus, T., 2016. Hierarchical bioinspired adhesive surfaces − A review. Bioinspiration & Biomimetics 11 (5), 051001.

[21] del Campo, A., Arzt, E., 2007. Design parameters and current fabrication approaches for developing bioinspired dry adhesives. Macromolecular Bioscience 7 (2), 118–127.

[22] Jeong, H.E., Kwak, M.K., Suh, K.Y., 2010. Stretchable, adhesion-tunable dry adhesive by surface wrinkling. Langmuir 26 (4), 2223–2226.

[23] Jeong, H.E., Kwak, R., Khademhosseini, A., Suh, K.Y., 2009. UV-assisted capillary force lithography for engineering biomimetic multiscale hierarchical structures: From lotus leaf to gecko foot hairs. Nanoscale 1 (3), 331–338.

[24] Aksak, B., Murphy, M.P., Sitti, M., 2007. Adhesion of biologically inspired vertical and angled polymer microfiber arrays. Langmuir 23 (6), 3322–3332.

[25] Huber, G., Gorb, S.N., Spolenak, R., Arzt, E., 2005. Resolving the nanoscale adhesion of individual gecko spatulae by atomic force microscopy. Biology Letters 1 (1), 2–4.

[26] Huber, G., Mantz, H., Spolenak, R., et al., 2005. Evidence for capillary contributions to gecko adhesion from single spatula nanomechanical measurements. Proceedings of the National Academy of Sciences of the United States of America 102 (45), 16293–16296.

[27] Autumn, K., Majidi, C., Groff, R.E., Dittmore, A., Fearing, R., 2006. Effective elastic modulus of isolated gecko setal arrays. Journal of Experimental Biology 209 (18), 3558–3568.

[28] Peattie Anne, M., Majidi, C., Corder, A., Full Robert, J., 2007. Ancestrally high elastic modulus of gecko setal β-keratin. Journal of The Royal Society Interface 4 (17), 1071–1076.

[29] Spolenak, R., Gorb, S., Gao, H., Arzt, E., 2005. Effects of contact shape on the scaling of biological attachments. Proceedings of the Royal Society A: Mathematical, Physical and Engineering Sciences 461 (2054), 305–319.

[30] Greiner, C., del Campo, A., Arzt, E., 2007. Adhesion of bioinspired micropatterned surfaces: Effects of pillar radius, aspect ratio, and preload. Langmuir 23 (7), 3495–3502.

[31] del Campo, A., Greiner, C., Arzt, E., 2007. Contact shape controls adhesion of bioinspired fibrillar surfaces. Langmuir 23 (20), 10235–10243.

[32] del Campo, A., Greiner, C., Álvarez, I., Arzt, E., 2007. Patterned surfaces with pillars with controlled 3D tip geometry mimicking bioattachment devices. Advanced Materials 19 (15), 1973–1977.

[33] Carbone, G., Pierro, E., Gorb, S.N., 2011. Origin of the superior adhesive performance of mushroom-shaped microstructured surfaces. Soft Matter 7 (12), 5545–5552.

[34] Balijepalli, R.G., Begley, M.R., Fleck, N.A., McMeeking, R.M., Arzt, E., 2016. Numerical simulation of the edge stress singularity and the adhesion strength for compliant mushroom fibrils adhered to rigid substrates. International Journal of Solids and Structures 85-86, 160–171.

[35] Li, M., Zhao, A., Jiang, R., et al., 2011. Regulation of the elastic modulus of polyurethane microarrays and its influence on gecko-inspired dry adhesion. Applied Surface Science 257 (8), 3336–3340.

[36] Lee, J., Fearing, R.S., Komvopoulos, K., 2008. Directional adhesion of gecko-inspired angled microfiber arrays. Applied Physics Letters 93 (19), 191910.

[37] Kim, T.-i., Jeong, H.E., Suh, K.Y., Lee, H.H., 2009. Stooped nanohairs: Geometry-controllable, unidirectional, reversible, and robust gecko-like dry adhesive. Advanced Materials 21 (22), 2276–2281.

[38] Majidi, C., Groff, R., Fearing, R., 2004. Clumping and packing of hair arrays manufactured by nanocasting. In: Proceedings of ASME International Mechanical Engineering Congress and Exposition (IMECE), pp. 579–584. California.

[39] Chung, J.Y., Chaudhury, M.K., 2005. Roles of discontinuities in bio-inspired adhesive pads. Journal of The Royal Society Interface 2 (2), 55–61.

[40] Geim, A.K., Dubonos, S.V., Grigorieva, I.V., et al., 2003. Microfabricated adhesive mimicking gecko foot-hair. Nature Materials 2, 461.

[41] Yao, H., Gao, H., 2006. Mechanics of robust and releasable adhesion in biology: Bottom–up designed hierarchical structures of gecko. Journal of the Mechanics and Physics of Solids 54 (6), 1120–1146.

[42] Northen, M.T., Turner, K.L., 2005. A batch fabricated biomimetic dry adhesive. Nanotechnology 16 (8), 1159–1166.

[43] Northen, M.T., Turner, K.L., 2006. Meso-scale adhesion testing of integrated micro- and nano-scale structures. Sensors and Actuators A: Physical 130-131, 583–587.

[44] Crosby, A.J., Hageman, M., Duncan, A., 2005. Controlling polymer adhesion with "pancakes". Langmuir 21 (25), 11738–11743.

[45] Sitti, M., Fearing, R.S., 2003. Synthetic gecko foot-hair micro/nano-structures as dry adhesives. Journal of Adhesion Science and Technology 17 (8), 1055–1073.

[46] Thomas, T., Crosby, A.J., 2006. Controlling adhesion with surface hole patterns. The Journal of Adhesion 82 (3), 311–329.

[47] Sameoto, D., Menon, C., 2009. A low-cost, high-yield fabrication method for producing optimized biomimetic dry adhesives. Journal of Micromechanics and Microengineering 19 (11), 115002.

[48] Yoon, E.-S., Singh, R.A., Kong, H., et al., 2006. Tribological properties of bio-mimetic nano-patterned polymeric surfaces on silicon wafer. Tribology Letters 21 (1), 31–37.

[49] Jeong, H.E., Lee, S.H., Kim, J.K., Suh, K.Y., 2006. Nanoengineered multiscale hierarchical structures with tailored wetting properties. Langmuir 22 (4), 1640–1645.

[50] Jin, M., Feng, X., Feng, L., et al., 2005. Superhydrophobic aligned polystyrene nanotube films with high adhesive force. Advanced Materials 17 (16), 1977–1981.

[51] Menon, C., Murphy, M., Sitti, M., 2004. Gecko inspired surface climbing robots. In: Proceedings of the 2004 IEEE International Conference on Robotics and Biomimetics, 22–26 August 2004, pp. 431–436.

[52] Khan, W., Sharma, R., Saini, P., 2016. Carbon nanotube-based polymer composites: Synthesis, properties and applications. In Carbon Nanotubes-Current Progress of Their Polymer Composites. InTech.

[53] Delzeit, L., Nguyen, C.V., Chen, B., et al., 2002. Multiwalled carbon nanotubes by chemical vapor deposition using multilayered metal catalysts. The Journal of Physical Chemistry B 106 (22), 5629–5635.

[54] Qu, L., Dai, L., Stone, M., Xia, Z., Wang, Z.L., 2008. Carbon nanotube arrays with strong shear binding-on and easy normal lifting-off. Science 322 (5899), 238–242.

[55] Yurdumakan, B., Raravikar, N.R., Ajayan, P.M., Dhinojwala, A., 2005. Synthetic gecko foot-hairs from multiwalled carbon nanotubes. Chemical Communications 30, 3799–3801.

[56] Sethi, S., Ge, L., Ci, L., Ajayan, P.M., Dhinojwala, A., 2008. Gecko-inspired carbon nanotube-based self-cleaning adhesives. Nano Letters 8 (3), 822–825.

[57] Ko, H., Zhang, Z., Ho, J.C., et al., 2010. Flexible carbon-nanofiber connectors with anisotropic adhesion properties. Small 6 (1), 22–26.

[58] Ko, H., Lee, J., Schubert, B.E., et al., 2009. Hybrid core–shell nanowire forests as self-selective chemical connectors. Nano Letters 9 (5), 2054–2058.

[59] Yu, D., Beckelmann, D., Opsölder, M., et al., 2018. Roll-to-roll manufacturing of micropatterned adhesives by template compression. Materials 12 (1), 97.

[60] Lee, S.H., Kim, S.W., Kang, B.S., Chang, P.-S., Kwak, M.K., 2018. Scalable and continuous fabrication of bio-inspired dry adhesives with a thermosetting polymer. Soft Matter 14 (14), 2586–2593.

[61] Hwang, I., Yi, H., Choi, J., Jeong, H.E., 2017. Fabrication of bioinspired dry adhesives by CNC machining and replica molding. International Journal of Precision Engineering and Manufacturing 18 (9), 1239–1244.

[62] Wirth, C.T., Hofmann, S., Robertson, J., 2008. Surface properties of vertically aligned carbon nanotube arrays. Diamond and Related Materials 17 (7), 1518–1524.

[63] Davies, J., Haq, S., Hawke, T., Sargent, J.P., 2009. A practical approach to the development of a synthetic Gecko tape. International Journal of Adhesion and Adhesives 29 (4), 380–390.

[64] Long, R., Hui, C.-Y., Kim, S., Sitti, M., 2008. Modeling the soft backing layer thickness effect on adhesion of elastic microfiber arrays. Journal of Applied Physics 104 (4), 044301.

[65] Sitti, M., Cusick, B., Aksak, B., et al., 2009. Dangling chain elastomers as repeatable fibrillar adhesives. ACS Applied Materials & Interfaces 1 (10), 2277–2287.

[66] Lee, J., Fearing, R.S., 2008. Contact self-cleaning of synthetic gecko adhesive from polymer microfibers. Langmuir 24 (19), 10587–10591.

[67] Parness, A., Soto, D., Esparza, N., et al., 2009. A microfabricated wedge-shaped adhesive array displaying gecko-like dynamic adhesion, directionality and long lifetime. Journal of The Royal Society Interface 6 (41), 1223–1232.

[68] Schubert, B., Lee, J., Majidi, C., Fearing, R.S., 2008. Sliding-induced adhesion of stiff polymer microfibre arrays. II. Microscale behaviour. Journal of The Royal Society Interface 5 (25), 845–853.

[69] Kim, T.-i., Pang, C., Suh, K.Y., 2009. Shape-tunable polymer nanofibrillar structures by oblique electron beam irradiation. Langmuir 25 (16), 8879–8882.

[70] Jeong, H.E., Lee, J.-K., Kim, H.N., Moon, S.H., Suh, K.Y., 2009. A nontransferring dry adhesive with hierarchical polymer nanohairs. Proceedings of the National Academy of Sciences of the United States of America 106 (14), 5639–5644.

[71] Murphy, M.P., Aksak, B., Sitti, M., 2009. Gecko-inspired directional and controllable adhesion. Small 5 (2), 170–175.

[72] Kendall, K., 1975. Thin-film peeling-the elastic term. Journal of Physics D: Applied Physics 8 (13), 1449–1452.

[73] Daltorio, K.A., Gorb, S., Peressadko, A., et al., 2006. A Robot that Climbs Walls using Micro-structured Polymer Feet. Berlin, Heidelberg: Springer Berlin Heidelberg, pp. 131–138.

[74] Sameoto, D., Menon, C., 2009. Direct molding of dry adhesives with anisotropic peel strength using an offset lift-off photoresist mold. Journal of Micromechanics and Microengineering 19 (11), 115026.

[75] Bauer, C.T., Kroner, E., Fleck, N.A., Arzt, E., 2015. Hierarchical macroscopic fibrillar adhesives:in situstudy of buckling and adhesion mechanisms on wavy substrates. Bioinspiration & Biomimetics 10 (6), 066002.

[76] Zhang, H., Wu, L., Jia, S., Guo, D., Dai, Z., 2012. Fabrication and adhesion of hierarchical micro-seta. Chinese Science Bulletin 57 (11), 1343–1349.

[77] Kang, S.M., 2016. Bioinspired design and fabrication of green-environmental dry adhesive with robust wide-tip shape. International Journal of Precision Engineering and Manufacturing-Green Technology 3 (2), 189–192.

[78] Seong, M., Lee, J., Hwang, I., Jeong, H.E., 2019. Significant adhesion enhancement of bioinspired dry adhesives by simple thermal treatment. International Journal of Precision Engineering and Manufacturing-Green Technology. 1–13.

[79] Kim, S., Sitti, M., Jang, J., Thomas, E.L., 2008. Fabrication of bio-inspired elastomer nanofiber arrays with spatulate tips using notching effect. Proceedings of the 2008 8th IEEE Conference on Nanotechnology, 18–21 August 2008, pp 780–782.

[80] Jin, K., Cremaldi, J.C., Erickson, J.S., et al., 2014. Biomimetic bidirectional switchable adhesive inspired by the gecko. Advanced Functional Materials 24 (5), 574–579.

[81] Wang, Z., 2018. Slanted functional gradient micropillars for optimal bioinspired dry adhesion. ACS Nano 12 (2), 1273–1284.

[82] Kizilkan, E., Gorb, S.N., 2018. Bioinspired further enhanced dry adhesive by the combined effect of the microstructure and surface free-energy increase. ACS Applied Materials & Interfaces 10 (31), 26752–26758.

[83] Wang, Y., Hu, H., Shao, J., Ding, Y., 2014. Fabrication of well-defined mushroom-shaped structures for biomimetic dry adhesive by conventional photolithography and molding. ACS Applied Materials & Interfaces 6 (4), 2213–2218.

[84] Ho, A.Y.Y., Yeo, L.P., Lam, Y.C., Rodríguez, I., 2011. Fabrication and analysis of gecko-inspired hierarchical polymer nanosetae. ACS Nano 5 (3), 1897–1906.

[85] Lee, D.Y., Lee, D.H., Lee, S.G., Cho, K., 2012. Hierarchical gecko-inspired nanohairs with a high aspect ratio induced by nanoyielding. Soft Matter 8 (18), 4905–4910.

[86] Lee, J., Majidi, C., Schubert, B., Fearing, R.S., 2008. Sliding-induced adhesion of stiff polymer microfibre arrays. I. Macroscale behaviour. Journal of The Royal Society Interface 5 (25), 835–844.

[87] Lee, H., Bhushan, B., 2012. Fabrication and characterization of hierarchical nanostructured smart adhesion surfaces. Journal of Colloid and Interface Science 372 (1), 231–238.
[88] Lee, J., Bush, B., Maboudian, R., Fearing, R.S., 2009. Gecko-inspired combined lamellar and nanofibrillar array for adhesion on nonplanar surface. Langmuir 25 (21), 12449–12453.
[89] Palacio, M.L.B., Bhushan, B., Schricker, S.R., 2013. Gecko-inspired fibril nanostructures for reversible adhesion in biomedical applications. Materials Letters 92, 409–412.
[90] Lu, G., Hong, W., Tong, L., et al., 2008. Drying enhanced adhesion of polythiophene nanotubule arrays on smooth surfaces. ACS Nano 2 (11), 2342–2348.
[91] Izadi, H., Golmakani, M., Penlidis, A., 2013. Enhanced adhesion and friction by electrostatic interactions of double-level Teflon nanopillars. Soft Matter 9 (6), 1985–1996.
[92] Izadi, H., Zhao, B., Han, Y., McManus, N., Penlidis, A., 2012. Teflon hierarchical nanopillars with dry and wet adhesive properties. Journal of Polymer Science Part B: Polymer Physics 50 (12), 846–851.
[93] Singh, R.A., Yoon, E.S., Kim, H.J., et al., 2007. Enhanced tribological properties of lotus leaf-like surfaces fabricated by capillary force lithography. Surface Engineering 23 (3), 161–164.
[94] Zhang, Y., Lin, C.-T., Yang, S., 2010. Fabrication of hierarchical pillar arrays from thermoplastic and photosensitive SU-8. Small 6 (6), 768–775.
[95] Maeno, Y., Nakayama, Y., 2009. Geckolike high shear strength by carbon nanotube fiber adhesives. Applied Physics Letters 94 (1), 012103.
[96] Rong, Z., Zhou, Y., Chen, B., et al., 2014. Bio-inspired hierarchical polymer fiber–carbon nanotube adhesives. Advanced Materials 26 (9), 1456–1461.
[97] Northen, M.T., Greiner, C., Arzt, E., Turner, K.L., 2008. A gecko-inspired reversible adhesive. Advanced Materials 20 (20), 3905–3909.
[98] Röhrig, M., Thiel, M., Worgull, M., Hölscher, H., 2012. 3D direct laser writing of nano- and microstructured hierarchical gecko-mimicking surfaces. Small 8 (19), 3009–3015.